TTC-Report 2008-07

SRF 080903-04
TESLA 2008

MAGNETIC FIELD ENHANCEMENT AT PITS AND BUMPS ON THE SURFACE OF SUPERCONDUCTING CAVITIES*

Valery Shemelin#, Hasan Padamsee
Laboratory for Elementary-Particle Physics, Cornell University, Ithaca, NY 14853

Abstract

One of the dominant causes of the large gradient spread and gradient limits in superconducting cavities is the abrupt quench of superconductivity due to "defects" on the surface. Many types of defects have been identified ([1], pp. 203-204). Some involve the presence of impurities. But there are also pure Nb defects such as pits and protrusions. We present results of calculations to show that the field enhancement factor for pits can reach the value of 4. We also calculate the magnetic field enhancement at the surface of ellipsoidal protrusions. This enhancement has a value of about 1.5 for a semispherical projection.

INTRODUCTION

With the progress of clean-room assembly and high-pressure rinsing, electric field limitations due to field emission and x-rays are coming under control to give gradients over 30 MV/m. However, many cavities demonstrate magnetic field limits leading to quench, which results in a large spread of maximum fields. The equator is the area with maximal magnetic field, and at the same time it is a place of the welded joint where the field can be enhanced at the irregularities up to the critical value. The critical magnetic field is the hard limit for the increase of the accelerating gradient. The way to higher gradients will depend strongly on the quality of the surface at the equatorial area.

Pits and protrusions lead to magnetic field enhancements which bring some parts of such features close to the theoretical maximum magnetic field. Figure 1, (a) and (b) shows two examples of pits found in SRF cavities many years ago [2, 3]. More recently advanced optical inspection techniques have shown pits or protrusions (c) in ILC 9-cell cavities that quench at about 15 MV/m (60 mT) [4].

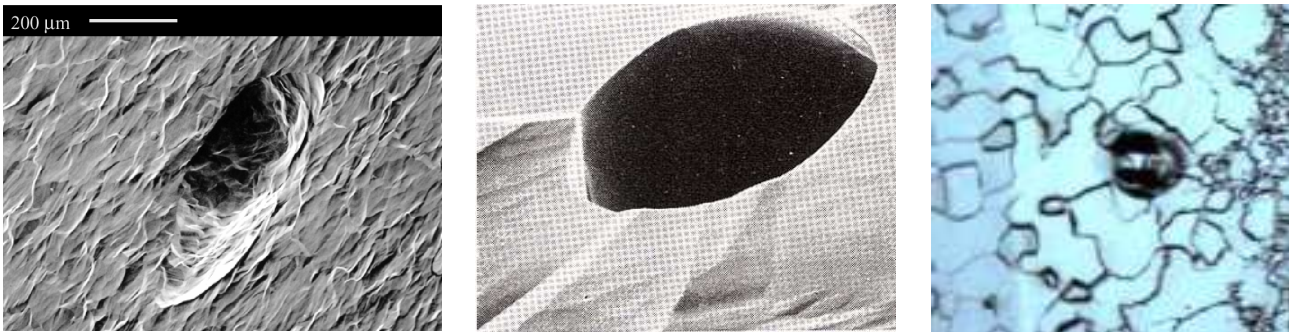

(a) (b) (c)

Figure 1. (a) A pit with sharp edge found in a 1.5 GHz cavity at a quench field of 93 mT [2]. (b) A weld hole found in a 3 GHz cavity [3]. The size of the pits can be estimated from the size of the nearby 50 – 100 um grains. (c) Protrusion found in an ILC 9-cell cavity using advanced optical inspection techniques [4].

FIELD ENHANCEMENT AT GRAIN BOUNDARY EDGES

Our work was first guided by the model of the magnetic field enhancement at grain boundaries [5] which attempted to explain in general terms the steep decline of the cavity quality (Q_0), i.e. the high field *Q*-slope. This model adopted a big variety of inter-grain boundaries. The maximal enhancement factor of 3 was obtained in calculations for 90° slope angle between grains. In the calculations of field enhancement at small steps on the wall made in [5], the 2-D finite element code SUPERLANS (or SLANS) [6] was used. This code calculates axially symmetric modes in an axially symmetric geometry. For calculations the TE_{011} mode was used, and the step was located on the round wall of a pill-box cavity.

The other version of this code, SLANS2, calculates modes with azimuthal variations, also in an axially symmetric geometry. We suppose that this code has high enough accuracy needed for analysis of small perturbations on the surface as well as SLANS has.

*Supported by NSF and DOE
#vs65@cornell.edu

CALCULATIONS OF FIELD ENHANCEMENT AT A PIT

For calculation of the magnetic field enhancement on a pit, this pit can be presented as a hole on the axis of a pill-box cavity with the mode TE_{111}. In Fig. 2, the picture of the current density (on the left) and of the magnetic field in the pill-box cavity with the pipes at the axis is shown. This picture was done with Microwave Studio®, 3-D code which gives a good interface but has not high enough accuracy for our purposes.

Figure 3 was obtained with SLANS2, and presents the magnetic field at two perpendicular cross-sections along the hole axis. The field is shown in one quarter of the cavity cross-section: on the right of the symmetry plane and above the axis of symmetry. Abscissa for the right-hand picture of Fig. 3 (and further, Fig. 9) is distance along the metal surface of the cavity from the equator till the axis.

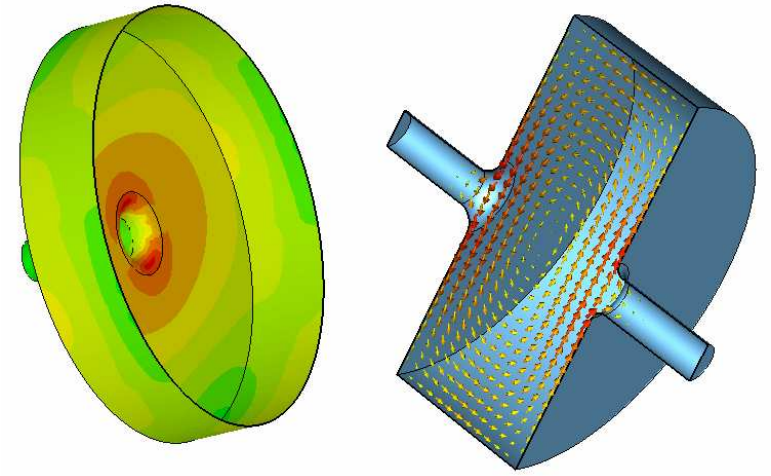

Figure 2. Current density on the surface of a pill-box cavity with beam-pipes, and magnetic field in its cross-section.

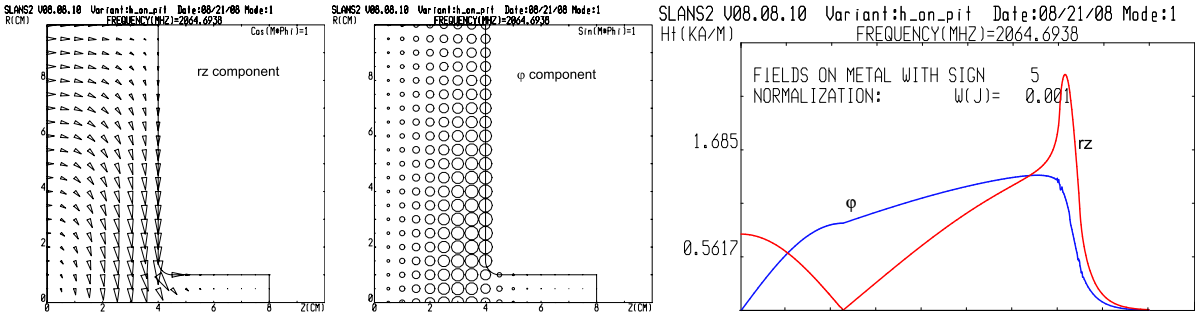

Figure 3. Magnetic field of a TE_{111} mode in a pill-box cavity with a pit at two mutually perpendicular cross-sections. On the right: field along the metal boundary, *rz* and φ components. Ratio of edge rounding to the pit radius is equal to $r/R = 1/2$, R = 10 mm.

The depth of the hole was several times bigger than its radius. In this case the result doesn't depend on the depth because the field drops very fast with the axial coordinate. For calculations of a real case, the size of the pit, Fig. 4, should be much less than the sizes of the cavity. At the same time, the radius of the edge rounding is a critical parameter in this calculation. To trace this dependences, calculations were performed for several values of r/R, taken from a series: $1/2$, $1/4$, $1/8$, $1/16$, and for a succession of decreasing radii of the hole: 10, 8, 6, 4, 2 mm by the cavity equator radius $R_{eq} = 100$ mm, results are presented in Fig. 5. Calculations for the same cavity without a hole were used for normalization of the obtained results. The limiting points of these curves ($R = 0$) corresponding to a very small pit compared to the sizes of the cavity, were found by quadratic extrapolation.

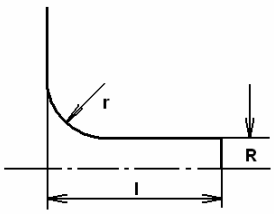

Figure. 4. Rounding radius, radius, and depth of the hole.

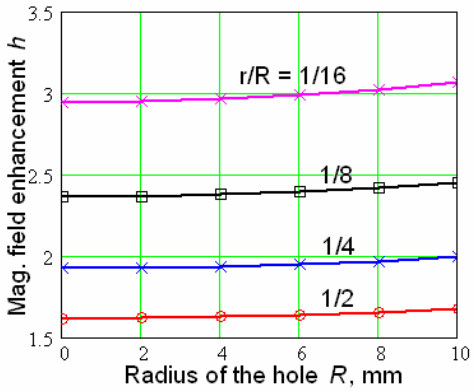

Figure 5. Enhancement of the magnetic field at the edge of a hole for different rounding radii *r* and hole radii *R*.

Then, these extrapolated points were plotted on the other graph, Fig. 6. Now, the ratio of the edge rounding radius to a pit radius was only taken into account. In the log-log graph, one can see that the power of dependence

$$h \propto (r/R)^n$$

changes from $n = -0.28$ for bigger values of *r/R* to approximately $n = -1/3$ for smaller *r/R*. Earlier results of numerical calculations [7] and theoretical analysis (with conformal mapping) for 2-D case [8] gave value of $n = -1/3$. In our case we have a transition from 3-D picture when *r* is comparable to *R*, to a 2-D picture for small *r/R*. So, extrapolation to small *r/R*'s should be done along the curve with $n = -1/3$. One can see that for a pit with a radius of 50 μm and the edge radius of 1 μm (*r/R* = 0.02) the field enhancement can reach a value >4 that is higher than values obtained for grain boundaries.

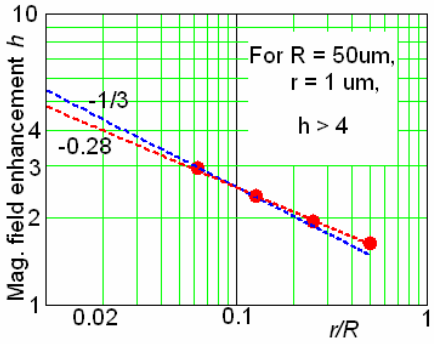

Figure 6. Enhancement of magnetic field for the hole sizes much less than the size of the cavity, for different *r/R*.

By the reasons discussed in [5] the effective radius of the edge is connected with a skin-layer thickness and is limited below by the value about 1 μm for the frequency of 1.3 GHz. So, we can not expect very high enhancement factor for small pits but a value above 4 is possible as the worst case. On the other hand, the measurements performed with an Atomic Force Microscope (AFM) on the edge of a grain boundary step show that corner radii of the order of 1 μm can exist, Fig. 7 [9].

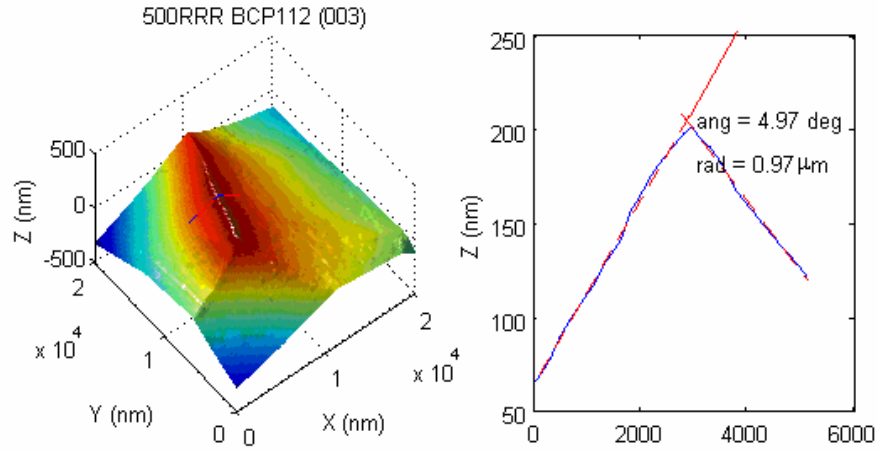

(a) (b)

Figure 7. (a) AFM image of a grain boundary edge. (b) A detailed analysis of the geometry of the step reveals the radius of curvature of the edge to be about 1 μm [9].

In the calculations presented above, the depth of the hole was several times bigger than its radius. In this case the result doesn't depend on the depth because the field drops very fast with the axial coordinate: as $\exp(-1.84\,z/r)$ (TE_{11} wave, very far below the cut-off), and at a distance equal to the pit diameter, it is equal to 2.5 % of the field at the upper side of the pit.

But even if the pit is shallow, field enhancement can be nevertheless high, for example, more than 90 % of maximal value for the pit having the ratio of depth to the hole radius $l/R = 0.5$, see designations in Fig. 4 and graph in Fig. 8.

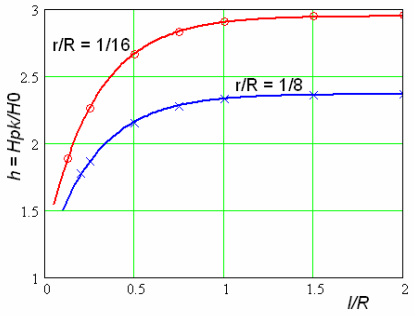

Figure 8. Field enhancement depending on the depth and rounding radius of the hole.

It is interesting to note that if the current could not flow into the pit, and the edge radius is zero, we should have the same 2-dimensional picture of magnetic field as the equipotentials of the electric field near the half-cylinder lying on a plane, with the same coefficient of enhancement: 2. Current flowing on both sides of the ridge is analogous to current on both sides of the ridge in the case of a grain boundary. This is a simplified explanation why the field is enhanced on the sharp ridge of a pit with a factor higher than 2.

Consistent results of the field calculations were obtained when the mesh used for this geometry had density smoothly increasing around the ridge area, Fig. 9.

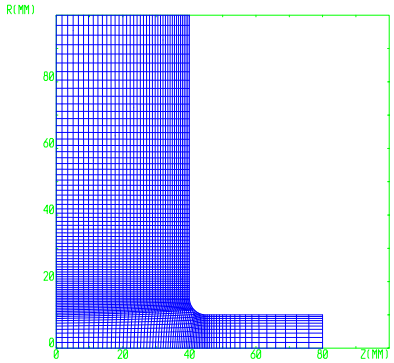

Figure 9. Example of a mesh for calculation fields at the cavity with a pit.

MAGNETIC FIELD ENHANCEMENT AT SEMIELLIPSOID ON A PLANE

Results of field enhancement calculations in [5] are verified by the example of a half-cylindrical protrusion on the plane which has a known enhancement factor equal to 2. Unfortunately, the author could not find an analytical solution for the enhancement of a magnetic field at the ellipsoidal or even spherical distortion of the surface. However, this case is adequate to our method, and moreover, has a practical interest, so it was analyzed also.

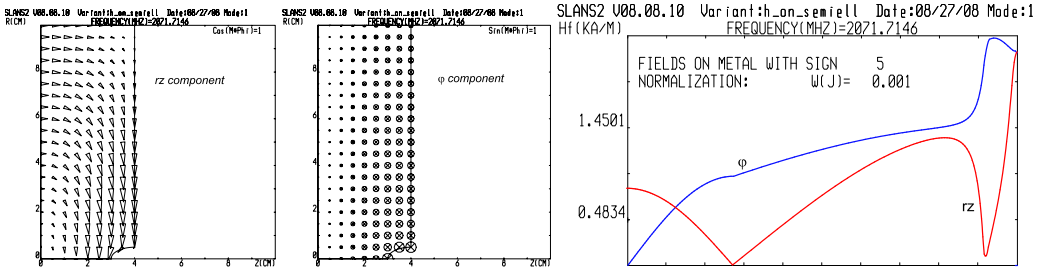

Figure 10. Magnetic field of a TE_{111} mode of a pill-box cavity with a semiellipsoidal protrusion at two mutually perpendicular cross-sections. On the right: field along the metal boundary, *rz* and φ components. Ratio of ellipsoid half-axis is $a/b = 1/2$, a = 10 mm

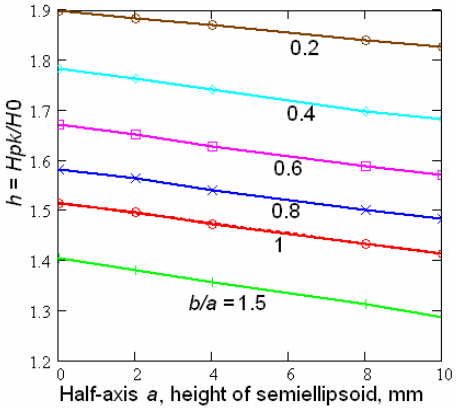

Figure 11. Magnetic field enhancement at the semiellipsoidal protrusion on a plane.

The picture of the magnetic field in presence of a big (for illustrative purpose) semiellipsoidal protrusion is shown in Fig. 10. One can see that the φ component has its maximum near the base of the semiellipsoid and the *rz* component is maximal at its top. Maximum of the φ component is bigger, and it is used below for calculation of the magnetic field enhancement. In calculations, again, values of half-axes were taken from a row of decreasing numbers: for the height of the protrusion a = 10, 8, 6, 4, and 2 mm, and for different ratios of half-axes *b/a*, Figure 11. Values for a very small height were found by extrapolation. Enhancement of magnetic field for the sizes of protrusion much less than the size of the cavity, is shown in Fig. 12. One can see that these values are not very big: about 1.5 for a semisphere, and about 2 for a very high semiellipsoid (whisker). But we should not forget that for two (or more) stacked defects – a small bump on a bigger one, or a crater on the tip of the semiellipsoidal protrusion, or a bump at the edge of the grain boundary – the enhancement factors multiply.

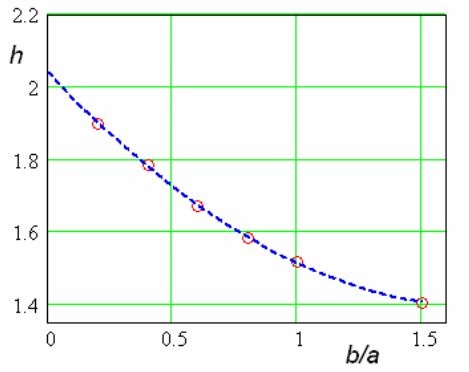

Figure 12. Magnetic field enhancement for different ratios of half-axes of a small semiellipsoid on a plane.

CONCLUSION

In development of the approach presented earlier [5], enhancement of magnetic field at round pits and protrusions on a flat surfaces was analyzed. For calculations, the SLANS2 code was used which calculates RF modes with azimuthal variations, instead of SLANS used in [5] used for axially symmetric modes. Presented results give numeric values for defects of the surface not evaluated in the previous work.

REFERENCES

1. H. Padamsee, J. Knobloch, T. Hays, *RF Superconductivity for Accelerators*, John Wiley & Sons, 1998.
2. J. Knobloch, *Advanced Thermometry Studies of Superconducting Radio-Frequency Cavities*, PhD Thesis, Cornell University, 1997.
3. H. Piel, *Superconducting Cavities*, CERN Accelerator School, May – June 1988, CERN 89-04, ed. S. Turner, p. 149 (1989).
4. Y. Iwashita et al. *Development of high resolution camera and observations of superconducting cavities.* EPAC08, Genoa, Italy.
5. J. Knobloch, R.L. Geng, M. Liepe, and H. Padamsee. *High-field Q slope in superconducting cavities due to magnetic field enhancement at grain boundaries.* SRF 1999, Santa Fe, NM.
6. D.G. Myakishev, V.P. Yakovlev. *The new possibilities of SuperLANS code for evaluation of axisymmetric cavities.* 1995 PAC and Int. Conf. on High-Energy Accel. May 1-5, 1995. Texas, pp. 2348-2350.
7. C. Reece. *Magnetic field enhancement at an inside corner of a cavity: Results of SUPERFISH calculations.* LEPP Report SRF-840302.
8. J. Amato. Private communication.
9. J. Shipman. *A Comparison of Grain Boundary Morphology of RRR 300 and RRR 500 Niobium After Various Polishing Processes, and Possible Implications for Q-Slope*, Master Thesis, Cornell University, 2004.